Hysteresis-based Charging Control of Plug-in Electric Vehicles

Soumya Kundu   Ian A. Hiskens

Abstract— The paper develops a hysteresis-based charging control strategy for plug-in electric vehicles (PEVs) that is capable of regulating charging load to satisfy system-wide services, including filling the overnight demand "valley" and balancing fluctuations in renewable generation. The actual state-of-charge (SoC) of a PEV battery follows a nominal SoC profile within a small hysteresis band. This leads to a sequence of ON and OFF cycles for the charger. The paper shows that in steady-state the probability distributions of SoC in the ON and OFF states, normalized around the nominal profile, follow a uniform distribution over the hysteresis deadband. Based on this steady-state behavior, a linearized state-space model has been developed to capture the response of aggregate electricity demand to shifts in the nominal SoC profile. A feedback control law is designed based on this linearized model.

I. INTRODUCTION

It has been estimated that by 2020, 25% of all automobile sales in the United States will be plug-in electric vehicles (PEVs) [1]. By then PEVs will account for 3%-6% of the total electricity demand. Unregulated charging of a large fleet of PEVs will introduce operational difficulties for the ageing and near-saturated grid infrastructure. On the other hand, regulating the charging process offers benefits for grid control. It is likely that most PEV charging will take place overnight when the non-PEV electricity demand is at its lowest (the "valley" hours) and wind generation is usually highest. If the charging of a large fleet of PEVs were to be regulated, it could serve a two-fold purpose, 1) fill the overnight demand valley thereby reducing daily cycling of power plants and the associated operational costs [2], and 2) encourage higher utilization of wind power by performing faster generation balancing [3], [4].

Many studies have investigated the feasibility and logistics of controlling electrical loads to perform generation balancing. Both centralized and decentralized control schemes have been investigated. Of particular relevance to this present work, [5] developed a hysteresis-based control strategy that enabled the aggregate power demand of a group of thermostatically controlled loads (TCLs) to follow fluctuations in wind power. It was shown that by applying small temperature setpoint changes uniformly across the population of TCLs, the net power consumption could be changed substantially. A tentative extension of this hysteresis-based control strategy to PEV charging was proposed in [4].

S. Kundu and I.A. Hiskens are with the Department of Electrical Engineering and Computer Science, University of Michigan, Ann Arbor, USA, (soumyak,hiskens@umich.edu).

N	number of PEVs
SoC	state-of-charge (kWh)
P_{max}	maximum charging rate (kW)
P_{nom}	nominal charging rate (kW)
E_{max}	battery charge capacity (kWh)
Δ	deadband width as a fraction of battery capacity
t_0	the instant when charging starts
t_f	the instant when charging completes

A linearized state-space model was developed in [6] to describe the aggregate response of a homogeneous group of TCLs to a shift in their temperature setpoints. In this paper, a similar approach is taken to model the collective behavior of PEV charging.

II. HYSTERESIS-BASED CHARGING

Hysteresis-based charging of a PEV battery assumes that charging takes place only at two allowed rates, either the charger draws power at its maximum rate P_{max} when it is 'ON', or it does not draw any power when it is 'OFF'. When the PEV charger draws power (in the ON state), the battery's state-of-charge (SoC), also a measure of the energy consumed, increases linearly. During the OFF state, the SoC remains constant. The charging process concludes when the SoC reaches the battery capacity E_{max}.

The sequence of ON and OFF states is determined by establishing a nominal charging trajectory and a small hysteresis band around that trajectory. In subsequent analysis it will be assumed that the width of the hysteresis band is the fraction Δ of the charge capacity for all PEVs. The SoC always stays within the hysteresis band. The nominal trajectory can be defined as the SoC profile if charging occurred at a constant rate P_{nom} throughout the charging duration. After the charging process starts (turns ON) at t_0, the charger turns OFF when its SoC touches the upper deadband limit, and remains OFF until its SoC touches the lower deadband limit. It then switches back to the ON state. This process continues until charging is completed at t_f. Fig. 1 shows a typical charging profile, with the left figure showing the entire charging process, and the right figure showing an enlargement of a section of that process.

The nominal charge profile over the duration of charging $[t_0, t_f]$, and the hysteresis deadband limits are given by,

$$SoC_{nom}(t) = (t - t_0)\,P_{nom}; \quad P_{nom} = \frac{E_{max}}{t_f - t_0} \quad (1a)$$

$$SoC_+(t) = (t - t_0)\,P_{nom} + E_{max}\Delta/2 \quad (1b)$$

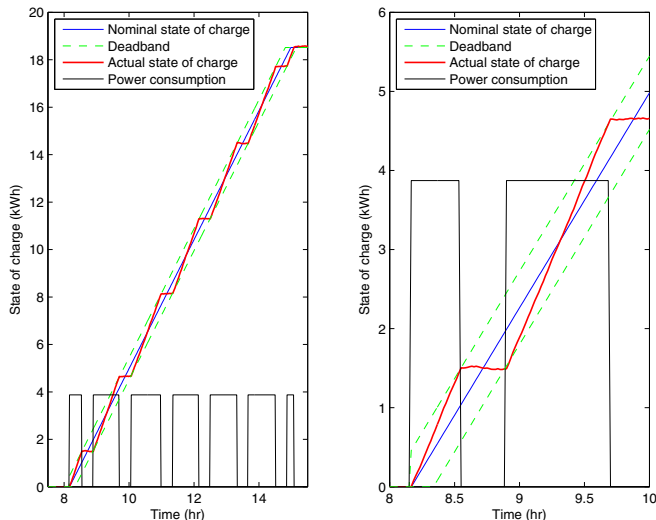$$SoC_-(t) = (t - t_0)\,P_{nom} - E_{max}\Delta/2. \quad (1c)$$

Fig. 1. Hysteresis-based charging profile.

If $s(t)$ denotes the state of a charger, with $s(t) = 1$ when ON and $s(t) = 0$ when OFF, then the dynamics governing the charging process can be expressed as,

$$\dot{SoC}(t) = s(t)P_{max} \qquad (2)$$

where

$$s(t) = \begin{cases} 1, & SoC(t) \leq SoC_{-}(t) \\ 0, & SoC(t) \geq SoC_{+}(t) \\ s(t-), & \text{otherwise.} \end{cases}$$

The deadband width for each vehicle is proportional to its maximum charge capacity, so the ratio of deadband width to charge capacity is the same for all PEVs. Defining the new variable

$$\widetilde{SoC}(t) := \frac{SoC(t) - SoC_{nom}(t)}{E_{max}}, \qquad (3)$$

which will be referred to as *normalized* SoC, the dynamics in (2) can be modified as,

$$\dot{\widetilde{SoC}}(t) = \frac{(s(t)P_{max} - P_{nom})}{E_{max}} \qquad (4)$$

where

$$s(t) = \begin{cases} 1, & \widetilde{SoC}(t) \leq -\Delta/2 \\ 0, & \widetilde{SoC}(t) \geq \Delta/2 \\ s(t-), & \text{otherwise.} \end{cases}$$

This formulation helps in normalizing the hysteresis deadband. While the actual deadband is time varying as it is centered around $SoC_{nom}(t)$, the normalized deadband is static, centered around zero, and has the same width Δ for all PEVs.

If all vehicles were to start charging at the same time t_0, the aggregate power demand would initially display large oscillations before ultimately settling to a steady-state aggregate demand, as shown in Fig. 2(a)[1]. To assist in

---

[1]For this example, the number of PEVs is $N = 20,000$. E_{max} was chosen to be uniformly distributed over the range 12-20 kWh and P_{max} to be uniformly distributed over 3-5 kW. The deadband width is the fraction $\Delta = 0.05$ of E_{max}.

understanding this load behavior, it is helpful to consider the evolution of the probability distribution of $\widetilde{SoC}(t)$ for PEVs in the ON state and those in the OFF state. These two distributions are shown in Figs. 2(b) and 2(c) respectively. Initially the ON-state probability distribution for $\widetilde{SoC}$ has a large peak slightly above zero. Over time, as PEVs charge, this peak moves toward the upper deadband limit $+\Delta/2$. When that limit is encountered, PEV charging ceases, so the peak migrates to the OFF-state distribution. The peak then moves steadily towards the lower deadband limit $-\Delta/2$, where it again migrates to the ON-state distribution. The peak decays after a few cycles due to heterogeneity, leading to the steady-state power demand shown in Fig. 2(a).

This oscillation can be avoided, however, if the starting instant is uniformly distributed over a time window of the same order as the duration of a typical ON/OFF charging cycle. Choosing t_0 to be uniformly distributed over a 50 minute time window largely attenuates the starting oscillations, as shown in Fig. 3(a). Figs. 3(b) and 3(c) show the corresponding evolution of the ON- and OFF-state probability distributions, starting from the instant when all the PEVs have begun charging.

III. LINEARIZED STATE-SPACE MODEL

The goal of the paper is to design a feedback controller that regulates the aggregate power demand of PEVs by varying the hysteresis deadband position while keeping the normalized width Δ fixed. This section develops a linearized state-space model of the system based on the steady-state probability distributions of chargers in the ON and OFF states. The approach is similar to that used in [6] to develop a state-space model of the response of a group of thermostatically controlled loads to shifts in the temperature deadband. Section III-A derives an expression for the steady-state probability distribution, while Section III-B builds a system model that is a linearization around that steady-state distribution. The analysis presented in this section is based on an assumption that the system is homogeneous and noise-free. However the Monte-Carlo simulation results presented later will consider a heterogenous system with noise.

A. Steady-state probability distribution

In steady-state, the aggregate power consumption becomes (*almost*, for non-homogeneous noisy systems) constant and hence the number of chargers in their ON state will be a constant N_{on}. Likewise, the number of chargers in the OFF state will also be constant, $N_{off} = N - N_{on}$. In steady-state, the number of chargers in the ON state and having a normalized SoC within the range $[\alpha, \beta]$, where $-\Delta/2 \leq \alpha < \beta \leq \Delta/2$, will be proportional to the time it takes to increase $\widetilde{SoC}$ from α to β. For chargers in the OFF-state, this would be the time it takes to decrease $\widetilde{SoC}$ from β to α. From (4), the time taken for a charger in the ON state to increase its $\widetilde{SoC}$ from α to β, with $\alpha, \beta \in [-\Delta/2, \Delta/2]$, would be proportional to the difference $(\beta - \alpha)$, and likewise for a charger in the OFF state, albeit with a different proportionality constant. Thus for both the
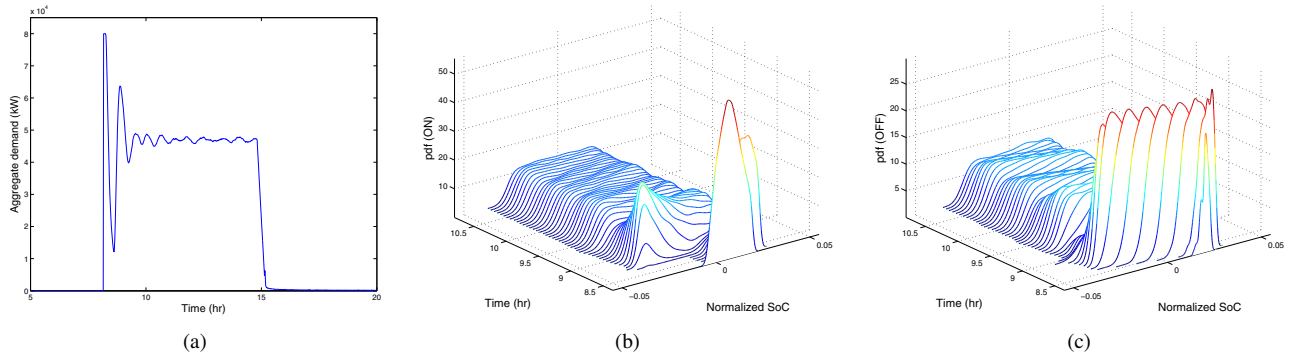
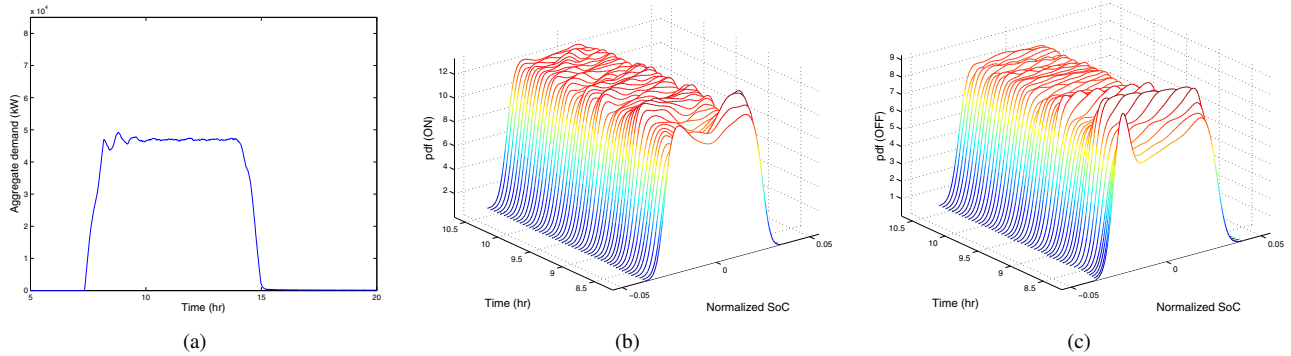Fig. 2. Aggregate response of hysteresis-based charging when the starting time is common for all PEVs.

Fig. 3. Aggregate response of hysteresis-based charging when the starting time is uniformly distributed.

ON and OFF states, the probability distributions are uniform over the range $[-\Delta/2, \Delta/2]$.

The values N_{on} and N_{off} can be found by equating the incoming and outgoing flux of probability at the boundaries of the normalized deadband $[-\Delta/2, \Delta/2]$. To maintain a steady-state distribution, the rate of departure of PEV chargers from the ON state should be equal to the rate of departure of chargers from the OFF state, so from (4),

$$N_{on}\frac{P_{max} - P_{nom}}{E_{max}} = N_{off}\frac{P_{nom}}{E_{max}}.$$

Using $N_{on} + N_{off} = N$ gives,

$$N_{on} = \frac{NP_{nom}}{P_{max}}, \qquad N_{off} = \frac{N(P_{max} - P_{nom})}{P_{max}},$$

and the probability density functions, f_{on} and f_{off} become,

$$f_{on} = \frac{P_{nom}}{P_{max}\Delta} \tag{5a}$$

$$f_{off} = \frac{P_{max} - P_{nom}}{P_{max}\Delta}. \tag{5b}$$

Fig. 4 shows how the probability distributions computed from (5) compare with the simulated steady-state distributions. The discrepancies could be attributed to the non-homogeneity and noise present in the simulated system.

B. Linearized step response

The response of an individual PEV to a step change in its hysteresis deadband will depend on where it is operating
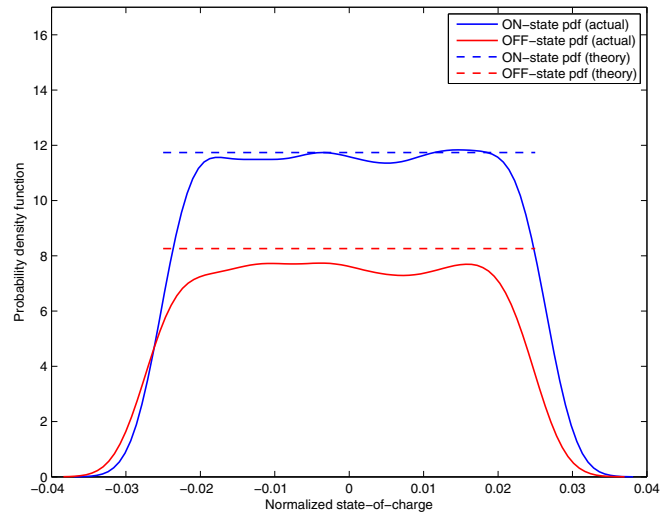

Fig. 4. Probability distribution of $\widetilde{SoC}$ for PEVs in the ON and OFF states.

in its ON/OFF cycle. Aggregating all such responses over a large population of PEVs establishes the desired step response of the entire load control scheme. Fig. 5 shows a typical step response for the aggregate demand. In order to build a linear model of this aggregate step response, the ON/OFF cycle will be divided into four cases, as shown in Fig. 6(a).
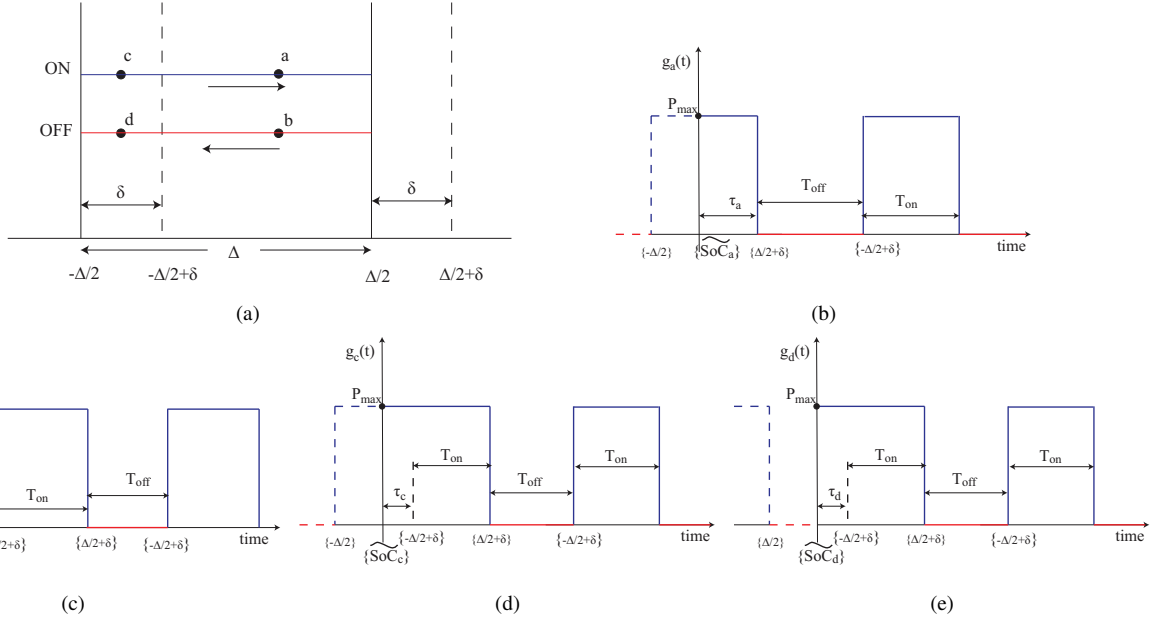
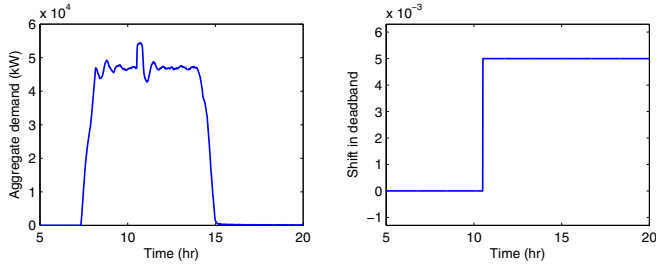Fig. 6. Individual responses to a shift in the hysteresis deadband.

Fig. 5. Response of aggregate demand to a step change in the deadband.

Fig. 7. Reference square-wave $g(t)$.

Point a: ON state, between $(-\Delta/2 + \delta)$ and $\Delta/2$: The response of a PEV charger lying in this region to the shift in the deadband would be similar to Fig. 6(b). Consider a charger at point 'a' in the ON state at the instant the shift is applied, having a normalized state-of-charge $\widetilde{SoC}_a \in [-\Delta/2 + \delta, \Delta/2]$. Without a shift it would have stayed ON until its $\widetilde{SoC}$ reached $\Delta/2$. But because of the shift, the upper limit of the deadband moves right to $\Delta/2 + \delta$. The charger will stay ON for some time τ_a, and then will continue with its natural OFF/ON sequence. Denote T_{on} and T_{off} as the time spent in the ON and OFF states respectively. Solving (4), we obtain

$$T_{on} = \frac{E_{max}\Delta}{P_{max} - P_{nom}}, \qquad T_{off} = \frac{E_{max}\Delta}{P_{nom}}. \qquad (6)$$

The power response $g_a(t)$ in Fig. 6(b) is a time-shifted version of the square waveform $g(t)$ in Fig. 7, where $g(t) = 0$ for $t < 0$. Denoting the Laplace transform of the reference waveform $g(t)$ as

$$\mathbf{G}(s) = \frac{P_{max}\left(1 - e^{-sT_{on}}\right)}{s\left(1 - e^{-s(T_{on}+T_{off})}\right)}, \qquad (7)$$

we obtain the Laplace transform $\mathbf{G}_a(s)$ of $g_a(t)$ as

$$g_a(t) = g(t + T_{on} - \tau_a)\mathbf{1}(t) ; \quad (\mathbf{1}(t) : \text{unit step})$$

$$\mathbf{G}_a(s, \tau_a) = e^{s(T_{on}-\tau_a)}\mathbf{G}(s) - \frac{e^{s(T_{on}-\tau_a)} - 1}{s}P_{max}$$

where

$$\tau_a = \frac{\Delta/2 + \delta - \widetilde{SoC}_a}{P_{max} - P_{nom}}$$

is the time taken to increase the normalized SoC from $\widetilde{SoC}_a$ to $\Delta/2 + \delta$.

Point b: OFF state, between $(-\Delta/2 + \delta)$ and $\Delta/2$: A charger sitting at point 'b' in the OFF state will respond to the shift in the manner shown in Fig. 6(c). Without the shift its normalized SoC would have decreased until $-\Delta/2$ before switching occurred. However under the shift its normalized SoC decreases from $\widetilde{SoC}_b$ to $-\Delta/2 + \delta$ in time τ_b and then continues on to the natural ON/OFF sequence. The waveform $g_b(t)$ is also a time-shifted version of $g(t)$ and has the Laplace transform

$$\mathbf{G}_b(s, \tau_b) = e^{-s\tau_b}\mathbf{G}(s) \qquad (8)$$

5601

where

$$\tau_b = \frac{\widetilde{SoC}_b + \Delta/2 - \delta}{P_{nom}} \qquad (9)$$

is the time taken for the normalized SoC to decrease from $\widetilde{SoC}_b$ to $-\Delta/2 + \delta$.

Point c: ON state, between $-\Delta/2$ and $(-\Delta/2 + \delta)$: A charger at point 'c' when the shift occurs will be below the lower deadband limit $(-\Delta/2 + \delta)$ and hence will have to charge for a time $(\tau_c + T_{on})$ to reach the upper deadband limit $\Delta/2 + \delta$. It will then continue onto its natural OFF/ON cycle. The Laplace transform of the power response in this case is given by,

$$\mathbf{G}_c(s, \tau_c) = e^{-s\tau_c}\mathbf{G}(s) + \frac{(1 - e^{-s\tau_c})}{s}P_{max} \qquad (10)$$

where

$$\tau_c = \frac{-\Delta/2 + \delta - \widetilde{SoC}_c}{P_{max} - P_{nom}} \qquad (11)$$

is the time taken to increase its normalized SoC from $\widetilde{SoC}_c$ to $-\Delta/2 + \delta$.

Point d: OFF state, between $-\Delta/2$ and $(-\Delta/2 + \delta)$: The response of a charger at point 'd' in the OFF state is distinct. While the chargers at points 'a', 'b' and 'c' do not immediately switch state, chargers in the region marked by 'd' are OFF at the instant the shift takes place and suddenly find their $\widetilde{SoC}$ below the new lower deadband limit $(-\Delta/2 + \delta)$. Hence they must immediately switch to the ON state. A typical response is shown in Fig. 6(e). The Laplace transform of this waveform is given by

$$\mathbf{G}_d(s, \tau_d) = e^{-s\tau_d}\mathbf{G}(s) + \frac{(1 - e^{-s\tau_d})}{s}P_{max} \qquad (12)$$

where

$$\tau_d = \frac{-\Delta/2 + \delta - \widetilde{SoC}_d}{P_{max} - P_{nom}} \qquad (13)$$

is the time taken to increase normalized SoC from $\widetilde{SoC}_d$ to $\Delta/2 + \delta$.

C. Aggregate response

The aggregate response of all the chargers in the four regions marked by 'a','b','c' and 'd' will be,

$$\mathbf{P}_a(s) = N\int_{-\Delta/2+\delta}^{\Delta/2} f_{on}\mathbf{G}_a(s, \tau_a) \, d\widetilde{SoC}_a \qquad (14)$$
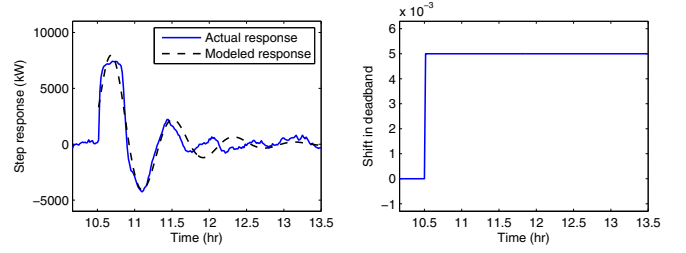
$$\mathbf{P}_b(s) = N\int_{-\Delta/2+\delta}^{\Delta/2} f_{off}\mathbf{G}_b(s, \tau_b) \, d\widetilde{SoC}_b \qquad (15)$$

$$\mathbf{P}_c(s) = N\int_{-\Delta/2}^{-\Delta/2+\delta} f_{on}\mathbf{G}_c(s, \tau_c) \, d\widetilde{SoC}_c \qquad (16)$$
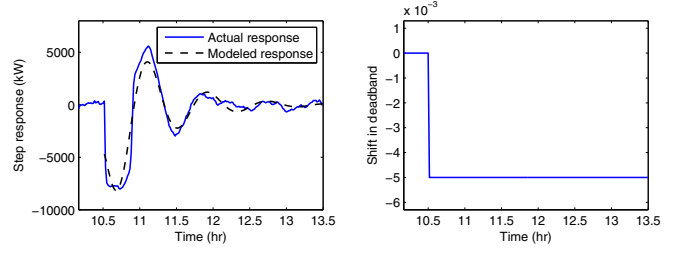
$$\mathbf{P}_d(s) = N\int_{-\Delta/2}^{-\Delta/2+\delta} f_{off}\mathbf{G}_d(s, \tau_d) \, d\widetilde{SoC}_d \qquad (17)$$

with the whole population's aggregate response given by,

$$\mathbf{P}_{tot}(s) = (\mathbf{P}_a(s) + \mathbf{P}_b(s) + \mathbf{P}_c(s) + \mathbf{P}_d(s)). \qquad (18)$$

(a) Step increase in the deadband.

(b) Step decrease in the deadband.

Fig. 8. Model performance compared with Monte-Carlo simulation.

Linearizing about the steady-state power consumption $P_{ss} = N_{on}P_{max}$ gives,

$$\widetilde{\mathbf{P}}_{tot}(s) = \mathbf{P}_{tot}(s) - \frac{P_{ss}}{s} \qquad (19)$$

$$\approx \left(\frac{I_0}{s + \sigma'} + \frac{A_\Delta}{(s+\sigma)^2 + \omega^2}\right)\delta \qquad (20)$$

with

$$I_0 = (P_{max} - P_{nom})N/\Delta \qquad (21)$$

$$\omega = \frac{2\sqrt{15}P_{nom}(P_{max} - P_{nom})}{\Delta\sqrt{P_{max}^2 + 2P_{nom}P_{max} - 2P_{nom}^2}} \qquad (22)$$

$$A_\Delta = \frac{10\sqrt{15}P_{nom}^2(P_{max} - P_{nom})^2 N}{\Delta(P_{max}^2 + 2P_{nom}P_{max} - 2P_{nom}^2)^{3/2}}, \qquad (23)$$

and where σ' and σ are damping parameters associated with heterogeneity and noise, which must be estimated in real-time[2]. The transfer function of the response is therefore given by,

$$\mathbf{T}(s) = \frac{s\,I_0}{s + \sigma'} + \frac{s\,A_\Delta}{(s+\sigma)^2 + \omega^2}. \qquad (24)$$

This is the response to a *right* shift in the deadband, where the nominal SoC profile increases. A similar analysis can be undertaken for a *left* shift, i.e. $\delta < 0$, in which case the transfer function has a similar form with $I_0 = P_{nom}N/\Delta$. Figs. 8(a) and 8(b) compare the model response with simulation results for a right and left shift of the deadband, respectively. The discrepancies in the two responses can be attributed to the non-homogeneity in the system.

[2]For the example system, estimation gives $\sigma' = 0.2$ and $\sigma = 0.025$.

IV. CONTROL DESIGN AND RESULTS

A. Control law

The system with transfer function (24) can be modeled in state-space form as,

$$\dot{x} = \mathbf{A}x + \mathbf{B}u \tag{25}$$

$$y = \mathbf{C}x + Du \tag{26}$$

where the input $u(t) \in \mathbb{R}$ is the shift in the deadband, and the output $y(t) \in \mathbb{R}$ is the displacement of the aggregate power demand from the steady-state value P_{ss}. The system is third order, with the state-space matrices are given by

$$\mathbf{A} = \begin{pmatrix} 0 & 0 & -\sigma'\left(\sigma^2 + \omega^2\right) \\ 1 & 0 & -\left(2\sigma\sigma' + \sigma^2 + \omega^2\right) \\ 0 & 1 & -\left(\sigma' + 2\sigma\right) \end{pmatrix}$$

$$\mathbf{B} = \begin{pmatrix} -I_0\sigma'\left(\sigma^2 + \omega^2\right) \\ A_\Delta\omega\sigma' - 2I_0\sigma\sigma' \\ A_\Delta - I_0\sigma' \end{pmatrix}$$

$$\mathbf{C} = \begin{pmatrix} 0 & 0 & 1 \end{pmatrix}$$

$$D = \begin{cases} (P_{max} - P_{nom})\,N/\Delta, & u(t) \le 0 \\ P_{nom}N/\Delta, & u(t) < 0. \end{cases}$$

To design the control law, a sliding surface $S(t)$ is defined,

$$S(t) := e(t) + c_i \int_0^t e(\tau)\,d\tau, \quad c_i > 0 \tag{27}$$

where

$$e(t) = y(t) - y_d(t), \tag{28}$$

and $y_d(t)$ is the trajectory describing the desired deviation in total demand from the steady-state value P_{ss}. The aim is to design a control input $u(t)$ that satisfies the relation,

$$\dot{S}(t) = -\eta S(t) \tag{29}$$

with $\eta > 0$. However because of the presence of the non-zero scalar D in (26), $\dot{S}(t)$ will include both $u(t)$ and $\dot{u}(t)$, as shown by manipulating (29) to give,

$$\dot{u}(t) + \left(c_i + \frac{\mathbf{CB}}{D}\right)u(t) = \frac{-\eta S(t) + \dot{y}_d(t) + c_i y_d(t)}{D}$$
$$- \frac{(\mathbf{CA} + c_i\mathbf{C})\,x(t)}{D}. \tag{30}$$

Thus instead of an algebraic equation for $u(t)$, (29) yields an ordinary differential equation in $u(t)$ and $\dot{u}(t)$. Deriving the control input $u(t)$ requires solution of (30), with initial condition obtained from,

$$e(0) = 0$$

$$\Rightarrow u(0) = \frac{y_d(0) - \mathbf{C}x(0)}{D}. \tag{31}$$

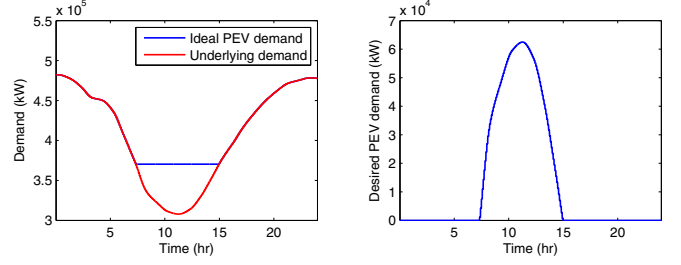A linear estimator is used to estimate the state $x(t)$ appearing in (30)-(31).

Fig. 9.   Ideal valley-filling profile.

B. Controller performance

Fig. 9 (left) shows a typical summer overnight base demand (scaled to suit our example) for the region managed by the Midwest Independent System Operator (MISO). The figure is time shifted to center the overnight period, with 0 hr. corresponding to 4:00pm. An ideal charging strategy would fill the overnight valley to achieve a flat demand curve, and at the same time ensure that all PEVs are fully charged by a stipulated time, say 8:00am which is 16 hr. in Fig. 9.

In order to generate the desired PEV demand trajectory y_d, it is assumed that each vehicle's required charge $E_{max,i}$ is known. Let $d(t)$ be the base (non-PEV) demand. Then the optimal *flat* demand level P_{des}, and the optimal charging start and completion time instants, t_0 and t_f, can be computed by iteratively solving the relation,

$$\int_{t_0}^{t_f} (P_{des} - d(t))\,dt = \sum_{i=1}^{N} E_{max,i}. \tag{32}$$

The valley-filling optimal PEV demand is then given by

$$y_d(t) = \begin{cases} P_{des} - d(t), & \text{if } t \in [t_0,\ t_f] \\ 0, & \text{otherwise} \end{cases} \tag{33}$$

as shown in Fig. 9 (right). An alternative approach to determining the optimal charging trajectory y_d is presented in [7]. In that case, all PEVs seek to minimize their charging costs, and in so doing achieve a Nash equilibrium that establishes the globally optimal charging trajectory.

Fig. 10 shows the closed loop performance of the controller for different reference trajectories and the corresponding control inputs. In Fig. 10(a) the aggregate PEV demand tracks the ideal valley-filling trajectory found in Fig. 9. Fig. 10(b) shows tracking of a reference trajectory which experiences a "step" decrease midway through the charging period. This situation could occur when there is a sudden increase in the non-PEV electricity demand or a sudden loss of a generator. In this case there is significant non-zero PEV demand beyond the optimal charge-completion time t_f. This non-zero power demand compensates for the reduced charging rates that occurred in response to the step decrease in the reference trajectory. In Fig. 10(c) the aggregate PEV demand tracks a fluctuating reference trajectory, possibly arising from wind generation.

It is interesting to note the large control input that's required towards the end of the charging process. This can
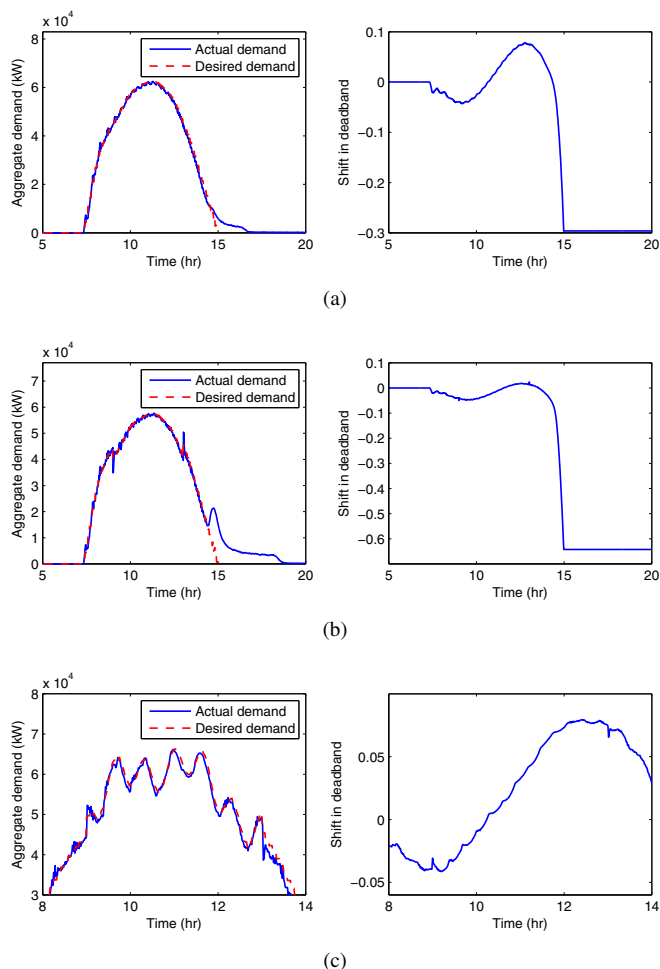
Fig. 10. Tracking performance of the controller in response to varying trajectories.

be attributed to the fact that as the charge completion time approaches, more and more vehicles become fully charged and hence take no further part in the closed loop control. This results in a loss of controllability.

V. CONCLUSIONS

This paper has considered aggregate control of a large population of plug-in electric vehicles (PEVs). A hysteresis-based charging strategy has been proposed, and a linearized model of the aggregate response of PEV chargers to a shift in the hysteresis deadband has been developed. This model forms the basis for a controller that enables load to respond to power system needs. A variety of examples have been considered, including load scheduling to achieve valley-filling, response to generator tripping, and tracking fluctuations in renewable generation. It has been observed that the controllability of the system is low towards the start and end of the charging duration. Further research is required to address these issues.

VI. ACKNOWLEDGEMENTS

The authors would like to thank Dr. Scott Backhaus and Dr. Nikolai Sinitsyn of Los Alamos National Laboratory for their helpful insights throughout this work.

REFERENCES

[1] S. Hadley, "Impact of plug-in hybrid vehicles on the electric grid", Technical Report ORNL/TM-2006/554, Oak Ridge National Laboratory, Oak Ridge, TN, October 2006.

[2] P. Denholm and W. Short, "An Evaluation of Utility System Impacts and Benefits of Optimality Dispatched Plug-in Hybrid Vehicles", Technical Report NREL-TP-620-40293, National Renewable Energy Laboratory, USA, October 2006.

[3] B. Kirby, "Spinning reserve from responsive loads", Technical Report ORNL/TM-2003/19, Oak Ridge National Laboratory, Oak Ridge, TN, March 2003.

[4] D.S. Callaway and I.A. Hiskens, "Achieving Controllability of Electric Loads", *Proceedings of the IEEE*, Vol. 99, No. 1, January 2011.

[5] D.S. Callaway, "Tapping the energy storage potential in electric loads to deliver load following and regulation, with application to wind energy", *Energy Conversion & Management*, 50(9):1389-1400, May 2009.

[6] S. Kundu, N. Sinitsyn, S. Backhaus and I.A. Hiskens, "Modeling and Control of Thermostatically-Controlled-Loads", *Proceedings of the 17th Power Systems Computations Conference*, Stockholm, Sweden, August 2011.

[7] Z. Ma, D.S. Callaway and I.A. Hiskens, "Decentralized charging control of large populations of plug-in electric vehicles", to appear *IEEE Transactions on Control Systems Technology*.